NCC 2020 Tutorial

Energy Harvesting and RF Energy Transfer aided Sustainable IoT Networks

Swades De

Department of Electrical Engineering
Communication Networks Research Group
Indian Institute of Technology Delhi

[ACKNOWLEDGMENT: Priyadarshi Mukherjee, Sharda Tripathi, Vini Gupta, Deepak Mishra, K Kaushik, Suraj Suman]

February 21, 2020

Presentation Outline

Energy Efficiency and Energy Harvesting

- A few methods are reported to assist the batteries to prolong the lifetime

Methods	Drawback
Medium Access Control (MAC)[33] Routing Protocols[34]	– improve node lifetime – do not ensure perpetual operation
Environmental Energy Sources[35] (solar, wind, ambient RF, $\cdots$ vibration, piezoelectric, etc.)	– random nature – unavailability in interior location – dimension of harvesting set-up

[33] P. Huang, L. Xiao, S. Soltani, M. W. Mutka, and N. Xi, "The evolution of MAC protocols in wireless sensor networks: A survey", *IEEE Commun. Surveys Tuts.*, vol. 15, no. 1, pp. 101–120, 2013.

[34] N. A. Pantazis, S. A. Nikolidakis, and D. D. Vergados, "Energy-efficient routing protocols in wireless sensor networks: A survey", *IEEE Commun. Surveys Tuts.*, vol. 15, no. 2, pp. 551–591, 2013.

[35] P. Kamalinejad, C. Mahapatra, Z. Sheng, S. Mirabbasi, V. C. M. Leung, and Y. L. Guan, "Wireless energy harvesting for the Internet of Things", *IEEE Commun. Mag.*, vol. 53, no. 6, pp. 102–108, 2015.

RF Energy Harvesting

- Network energy harvesting[36,37]
- Integrated data and energy mule[38]
- Multi-hop and multi-path RF energy transfer[39,40,41,42]
- Charging time characterization[43,44]
- Optimum relay placement[45]

---

[36] S. De et al. (Proc. IEEE ICC 2010)
[37] S. De and S. Chatterjee (IGI book chapter 2011)
[38] S. De and R. Singhal (IEEE Computer Mag., 45(9), 2012)
[39] P. Gupta et al. (Proc. NCC 2013)
[40] K. Kaushik et al. (Proc. IEEE PIMRC 2013)
[41] D. Mishra et al. (Proc. IEEE PIMRC 2014)
[42] D. Mishra et al. (IEEE Commun. Mag., 53(4), 2015)
[43] D. Mishra et al. (IEEE TCAS-II, 62(4), 2015)
[44] D. Mishra and S. De (IEEE Access J., vol. 4, 2016)
[45] D. Mishra and S. De (IEEE TCOM, 63(5), 2015)

Energy Harvesting Communication Networks

- Optimization on joint information and RF energy transfer[46,47]
- Relay-powered RF Harvesting WSN (RPCN)[48,49]
- Optimal time allocation for RFET and WIT in RPCN[50]
- Low-cost RF harvesting based wakeup receiver[51,52]

[46] D. Mishra and S. De (Prof. IEEE ICC, 2016)

[47] D. Mishra et al. (IEEE TCOM, 64(2), 2016)

[48] D. Mishra and S. De (Proc. IEEE CCNC, 2016)

[49] D. Mishra and S. De (Proc. Nat. Conf. Commun., 2016)

[50] D. Mishra and S. De (IET Electron. Lett., 2016)

[51] K Kaushik et al. (Proc. IEEE Sensors Conf., 2015)

[52] K Kaushik et al. (IEEE Sensors J., 2016)

Architecture for Network RF Energy Harvesting [53]

Motivation

In a homogeneous network a node cannot sustain solely from network RF energy

Two tier network architecture

Tier-1: **Energy constrained field nodes** with rudimentary communication

Tier-2: Relatively **powerful router/cluster-head nodes**

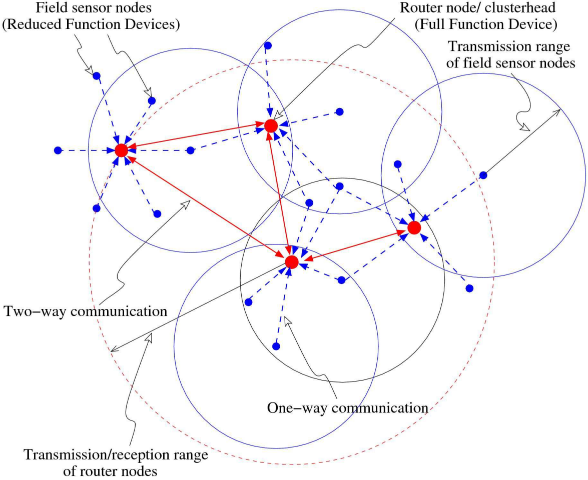

[53] S. De, A. Kawatra, and S. Chatterjee, "On the feasibility of network energy operated field sensors," in *Proc. IEEE Intl. Conf. Commun.* (ICC), Cape Town, South Africa, May 2010.

Energy Availability versus Activity Cycle

- For tier-1 nodes, to preserve energy long sleep duration is required and to replenish lost energy it requires sufficient ambient network RF energy

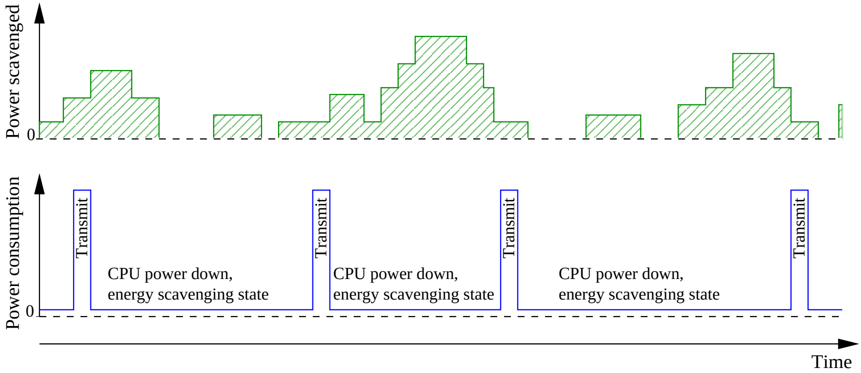

- A stable condition can be achieved by operating tier-2 nodes with uninterrupted power supply (nodal mobility or external energy source)

Available Network RF Energy (I)

Depends on the simultaneous transmitters as well as their positions relative to the harvester node

Lemma 1 (1)

In a CSMA/CA wireless network with homogeneous communication coverage, with finite node density the maximum number of simultaneously transmitting neighboring nodes is limited to 5.

$$n_t = \left\lfloor \frac{2\left(\pi - \arccos \frac{d_s}{2R_C}\right)}{\frac{\pi}{3}} \right\rfloor + 2$$

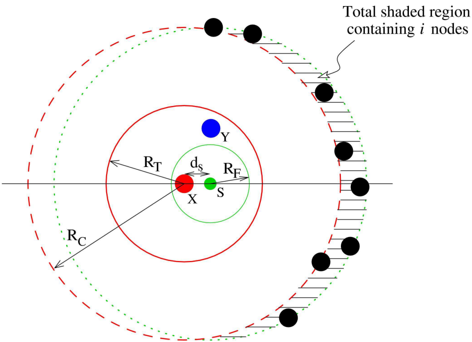

Corollary 2 (1)

n_t *is maximum* $(= 5)$ *when* $d_S = R_F \approx \frac{R_C}{4}$

Available Network RF Energy (II)

Lemma 3 (2)

More number of simultaneous transmissions around a harvester node does not imply more energy available for harvesting.

Corollary 4 (2)

The maximum power for harvesting is available when the harvester is located closest to a transmitter. Total conditional average power available at S is given by:

$$P_{s|X}(d_s) = k\frac{P_t}{d_s^{\gamma}} + \sum^{\infty} \sum^{\min\{i,4\}} p(i)P_{ij}(A)$$

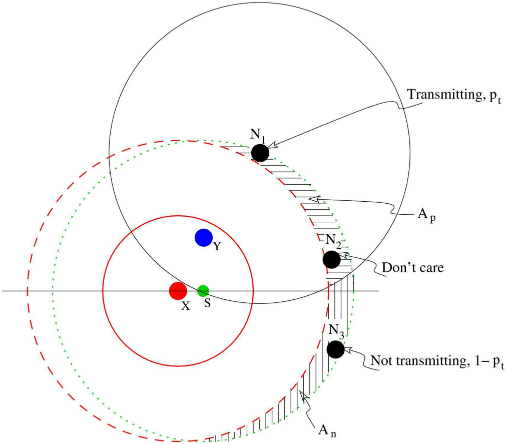

Effective RF Harvesting Energy Gain: Proof of concept

RF energy harvesting gain

- Tier-1 nodes: data of low power CPU and transceiver
- Tier-2 nodes (CC2520) transmit with probability 0.3, at 5 dBm output power
- Data frame length 40 Byte; transmission speed 250 kbps; frequency = 915 MHz
- $T_{sleep} = \frac{E_{\text{on}}}{P_s^{(\text{scv})} - P_{\text{leak}}}$ where

$$P_s^{(\text{scv})} = \eta p_{\text{tr}} \sum_{d_s^{(l)}}^{d_s^{(u)}} \Pr(d_s) P_{s|X}(d_s)$$

Condition on duty cycle

- Limit on sustainable transmission duty cycle for a given transmitter-to-harvester distance at various rectification efficiency for $ptr = 0.3$ and $P_{leak} = 30$ pW.

Energy hatvesting gain at $\eta = 0.06\%$

Rectification effy. at 30pW leakage (%)	Avg. sleep duration (min)	Leakage power at rect. effy. of 1% (pW)	Avg. sleep duration (min)
1	142	0	13.36
2	69	30	13.44
5	27	1	16.55
10	13.44	10,000	infeasible

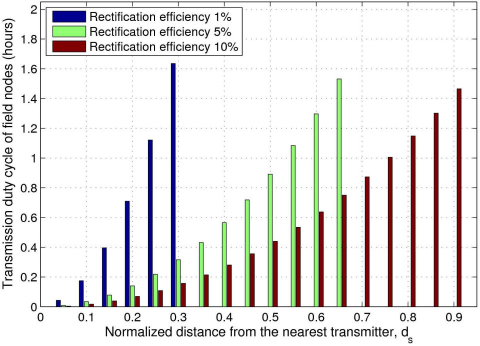

Limitations of Conventional Direct RF Energy Transfer

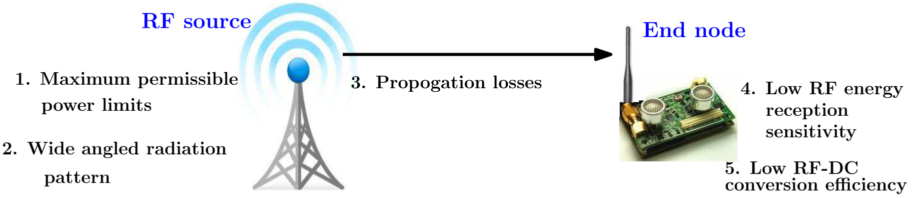

Goal: Novel node level and network level strategies to **boost RF-ET efficiency** and support **uninterrupted network operation**

First Proposal: Novel “packetized" energy communication schemes: **Multihop RF energy transfer** and **multi-path energy routing**

Robot-assisted Charging Framework

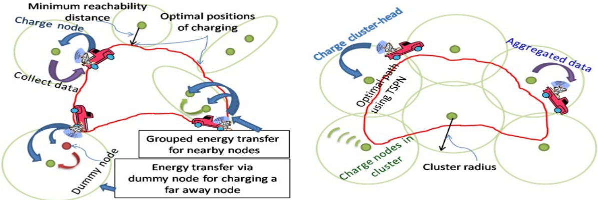

Figure 1: Integrated Data and Energy Mule (IDEM)[54]

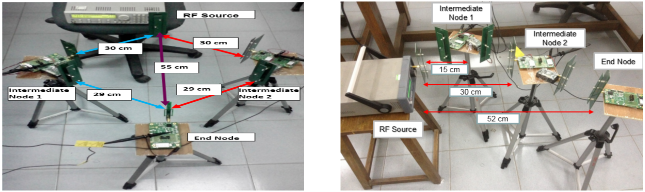

Figure 2: Demonstration of multi-path energy routing (MPER)[55]

[54] S. De and R. Singhal, "Toward uninterrupted operation of wireless sensor networks", *IEEE Comp. Mag.*, vol. 45, no. 9, pp. 24–30, 2012.

[55] D. Mishra, S. De, S. Jana, S. Basagni, K. Chowdhury, and W. Heinzelman, "Smart RF energy harvesting communications: Challenges and opportunities", *IEEE Commun. Mag.*, vol. 53, no. 4, pp. 70–78, 2015.

Perpetual Network Operation

- iDEM$\leftarrow$ mobile data collection and recharging
- Charging time and iDEM revisit time characterization
- Renewable energy cycle $\leftarrow$ charging time and iDEM revisit time
- Considering practical supercapacitor models
- Leakage, self-discharge, and aging effects
- Accurately estimating performance of green energy harvesting sensor networks

iDEM scheduling

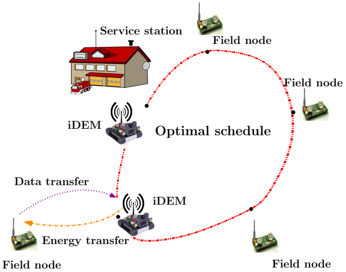

Renewable energy cycle

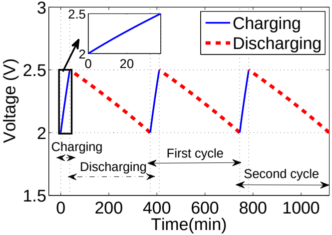

Limitations of Terrestrial RFET

- Energy harvesting from dedicated energy source
- Wireless power transfer (WPT)[56] is reliable
- Battery can be recharged in periodic manner through WPT

Methods	**Drawback**
Static setup[57]	– fixed infrastructure needed – electric power supply provisioning – expensive
Ground Vehicles (Robot)	– lack of path availability – well-furnished environment required – reachability to sensor nodes

[56] L. Xie *et al.*, "Wireless power transfer and applications to sensor networks", *IEEE Wireless Commun.*, vol. 20, no. 4, pp. 140–145, 2013.

[57] H. Dai, Y. Liu, G. Chen, X. Wu, T. He, A. X. Liu, and H. Ma, "Safe charging for wireless power transfer", *IEEE/ACM Trans. Netw.*, vol. 25, no. 6, pp. 3531–3544, 2017.

UAV-aided RFET

- Advantages of UAV-aided RFET:

excellent maneuvering	accessibility to almost all locations
cost-effective	remote controlled and programming flexibility
on-demand service	sufficient payload carrying capability

- For WPT, *RFET* is preferred over *magnetic resonance coupling (MRC)*

	RFET	**MRC**
Range	efficiency $\downarrow$ with distance	very limited (a few cm)
Alignment	not required	stringent
Vibration	insensitive	highly sensitive

- Also, unlike in MRC, *information* as well as *power* can be transferred over the same wave in RFET[58]

[58] B. Clerckx, R. Zhang, R. Schober, D. W. K. Ng, D. I. Kim, and H. V. Poor, "Fundamentals of wireless information and power transfer: From RF energy harvester models to signal and system designs", *IEEE J. Sel. Areas Commun.*, vol. 37, no. 1, pp. 4–33, 2019.

Path Loss Model for UAV-aided RFET

- Path loss model for UAV-aided communication architecture in different deployment scenarios:
  - High altitude platform in suburban/urban[59] (hovering altitude ≈ km)
  - Low altitude platform in suburban/urban[60] (hovering altitude ≈ 100 m)
  - Over-water scenario[61] (hovering altitude ≈ km)
  - Hilly and mountainous scenario[62] (hovering altitude ≈ km)

- UAV-aided RFET is facilitated at *very low altitude (up to a few meters)* due to low energy reception sensitivity
- Height of scatterer is mostly higher than hovering altitude
- Fresh investigation of path loss model for UAV-aided RFET

[59] J. Holis and P. Pechac, "Elevation dependent shadowing model for mobile communications via high altitude platforms in built-up areas", *IEEE Trans. Antennas and Propag.*, vol. 56, no. 4, pp. 1078–1084, 2008.

[60] A. Al-Hourani, S. Kandeepan, and A. Jamalipour, "Modeling air-to-ground path loss for low altitude platforms in urban environments", in *Proc. IEEE Global Commun. Conf.*, 2014, pp. 2898–2904.

[61] D. W. Matolak and R. Sun, "Air–ground channel characterization for unmanned aircraft systems—part i: Methods, measurements, and models for over-water settings", *IEEE Trans. Veh. Technol.*, vol. 66, no. 1, pp. 26–44, 2017.

[62] R. Sun and D. W. Matolak, "Air–ground channel characterization for unmanned aircraft systems part ii: Hilly and mountainous settings", *IEEE Trans. Veh. Technol.*, vol. 66, no. 3, pp. 1913–1925, 2017.

Path Loss Model (Contd.)

- Path loss is modeled for following deployment scenarios:
  suburban, urban, dense-urban, high-rise urban
- *ITU-R* recommendations are used to realize them[63]
- Ray propagation is simulated on *Wireless Insite* software[64]

- Receivers are placed on ground separated from each other by 0.5 m
- Transmitter are placed at different altitude from 1 m to 5 m

- Large-scale fading is of interest
  - RFET is facilitated over long time duration (up to several minutes)
  - Multipath fading is averaged out

[63] *Propagation data and prediction methods for the planning of short-range outdoor radiocommunication systems and radio local area networks in the frequency range 300 MHz to 100 GHz*, Recommendation ITU-R P.1411-9, 2017.

[64] (). Wireless insite, [Online]. Available: https://www.remcom.com/wireless-insite-em-propagation-software/.

Path Loss Model (Contd.)

- Path loss experienced at the k^{th} position L_k^{cal} is given by:

$$L_k^{cal} = 10\log_{10}(P_{tx}) - 10\log_{10}(P_{rx_k}) \quad [\text{in dB}]$$

where P_{tx}: power transmitted by transmitter mounted on UAV
P_{rx_k}: received power at the k^{th} position

- Excess path loss at the k^{th} position $(\mathcal{X}_k)$ is defined as:

$$\mathcal{X}_k \triangleq L_k^{cal} - L_k^{fs} \qquad [\text{in dB}].$$

where L_k^{fs} is the free space path loss obtained from Friis equation:

$$L_k^{fs} = 20\ \log_{10}(l_k) + 20\ \log_{10}(4\pi f/c)$$

l_k: distance between transmitter and k^{th} receiver
f: frequency of transmitted signal
c: speed of light

Path Loss Model (Contd.)

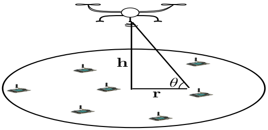

- Excess path loss is modeled as a function of elevation angle θ
- The excess path loss for each θ is separately computed
- Its variation found to closely follow Normal distribution and modeled as:

$$\mathcal{X} \sim \mathcal{N}\Big(\mu(\theta), \sigma^2(\theta)\Big)$$

- The mean $\mu(\theta)$ (in dB) and variance $\sigma^2(\theta)$ (in dB) vary as:

$$\mu(\theta) = a \cdot \exp(b \cdot \theta), \quad \sigma^2(\theta) = c \cdot \exp(d \cdot \theta)$$

Total path loss = Free space path loss + excess path loss $\Rightarrow L = L_{fs} + \mathcal{X}$

Path Loss Model (Contd.)

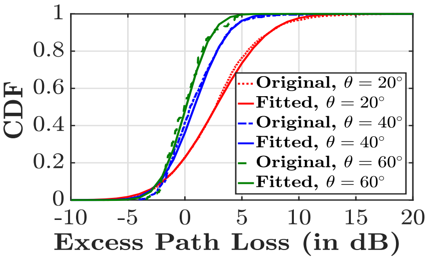

Figure 3: CDF of excess path loss at different elevation angle

Table 1: Values of empirical parameters of excess path loss for different scenarios

Environment	a	b	c	d
Suburban	12.05	−0.0742	79.24	−0.0817
Urban	22.09	−0.0430	652.47	−0.1037
Dense urban	28.74	−0.0558	702.23	−0.0782
High-rise urban	46.39	−0.0482	806.21	−0.0384

Path Loss Model (Contd.)

(a) suburban (b) agriculture

Figure 4: Experimental setup for validation of UAV-aided RFET path loss model

System Model

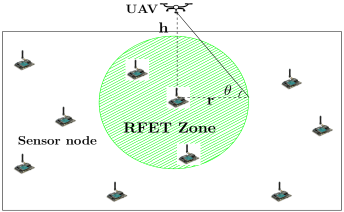

Figure 5: System model for UAV-aided charging

Path loss is modeled as:

$$L(h,\theta) = L_{fs}(h,\theta) + \mathcal{X}$$

θ is elevation angle made at the sensor node

$L_{fs}(h,\theta) = 20\log_{10}(h \cdot \csc\theta) + 20\log_{10}(f) - 10\log_{10}(G_{tx}G_{rx}) + 32.44$

$\mathcal{X}$ is the excess path loss: $\mathcal{X} \sim \mathcal{N}(\mu(\theta), \sigma^2(\theta))$

$$\mu(\theta) = a \cdot \exp(b \cdot \theta), \quad \sigma^2(\theta) = c \cdot \exp(d \cdot \theta)$$

For suburban area, the parameter values are:

$a = 12.05, b = -0.0742, c = 79.24, d = -0.0817$

Formation of RFET Zone

RFET zone is the ground field area within which the sensors are able to harvest energy from the RF wave transmitted from UAV

For RFET zone, the received power in expected sense is:

$$\mathbb{E}[P_{rx}(h,\theta)] \geq P_o \Rightarrow \mathbb{E}[L(h,\theta)] \leq P_{tx} - P_o$$

where P_{tx}: transmitted power
$P_o = -12$ dBm: sensitivity of energy harvester

Theorem 5

The expected value of path loss is not a convex function of height and radius.

Lemma 6

The path loss is unimodal function of height (altitude) for a given radius.

Lemma 7

The path loss is a non-decreasing function of radius for a given altitude.

Effective Power Harvested at Field Sensor Node

- The harvested power $P_{\mathcal{H}}(\rho)$ is found to vary with input received power ρ

$$P_{\mathcal{H}}(\rho) = \begin{cases} 0, & \text{if } \rho < \rho_o \\ \sum_{i=0}^{2} w_i \cdot \rho^i, & \text{otherwise} \end{cases}$$

where $\rho_o = 10^{\frac{P_o}{10}}$ W; w_i's are fitting coefficients having values $w_0 = -4.858 \times 10^{-5}$, $w_1 = 0.5875$, $w_2 = -7.564$

- The harvested power $P_{sen}(h, \theta)$ at a sensor node making an elevation angle θ with the UAV hovering at altitude h is:

$$\begin{aligned} P_{sen}(h, \theta) &= \int_{\rho \geq \rho_o} (w_0 + w_1 \cdot \rho + w_2 \cdot \rho^2) \cdot f_{P_{rx}(h,\theta)}(\rho) \cdot d\rho \\ &= \eta_0 + \eta_1 + \eta_2 \end{aligned}$$

where $f_{P_{rx}(h,\theta)}(\rho)$ denotes the distribution of received power:

$$f_{P_{rx}(h,\theta)}(\rho) = \frac{10}{\rho\sqrt{2\pi}\sigma(\theta)\ln(10)} \exp\left[-\frac{(10\log_{10}(\rho) - P_{tx} + L_{fs}(h,\theta) + \mu(\theta))^2}{2\sigma^2(\theta)}\right]$$

Effective Power Harvested (Contd.)

η_0, η_1, and η_2 are obtained as:

$$\eta_0 = w_0 \cdot Q(\kappa_0), \text{with } \kappa_0 = \frac{10\log_{10}\rho_o - P_{tx} + L_{fs}(h,\theta) + \mu(\theta)}{\sigma(\theta)}$$

$$\eta_1 = w_1 \cdot \exp\left[(P_{tx} - L_{fs}(h,\theta) - \mu(\theta)) \cdot \frac{\ln 10}{10} + \frac{\sigma^2(\theta)}{2}\left(\frac{\ln 10}{10}\right)^2\right] \cdot Q(\kappa_1)$$

$$\text{with } \kappa_1 = \frac{10\log_{10}\rho_o - P_{tx} + L_{fs}(h,\theta) + \mu(\theta) - \frac{\sigma^2(\theta)\ln 10}{10}}{\sigma(\theta)}$$

$$\eta_2 = w_2 \cdot \exp\left[2(P_{tx} - L_{fs}(h,\theta) - \mu(\theta))\frac{\ln 10}{10} + \frac{\sigma^2(\theta)}{2} \cdot \left(\frac{2\ln 10}{10}\right)^2\right] \cdot Q(\kappa_2)$$

$$\text{with } \kappa_2 = \frac{10\log_{10}\rho_o - P_{tx} + L_{fs}(h,\theta) + \mu(\theta) - 2\frac{\sigma^2(\theta)\ln 10}{10}}{\sigma(\theta)}$$

UAV Mobility Optimization

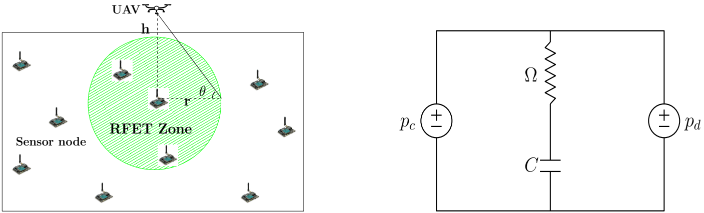

Figure 6: System model for UAV-aided charging and depiction of circuit operation at sensor node

- UAV charges each sensor nodes by hovering just above it
- N_S sensor nodes are deployed in a given area A
- k^{th} sensor node having initial voltage v_I^k and energy dissipation rate p_d^k
- UAV hovers above k^{th} sensor node for duration t_k
- Nodes are charged for target operation time T

UAV Mobility Optimization (Contd.)

$$(\mathbf{P}): \underset{t_i,\, x_{ij}}{\text{minimize}} \quad \sum_{i=1}^{N_S} t_i + \frac{1}{\mathcal{U}} \sum_{i=1}^{N_S} \sum_{j=1}^{N_S} x_{ij} d_{ij}$$

subject to:

$$(C1) \quad v_F^k(v_I^k, \underline{p}^k, \underline{t}) \geq v_{th}^k, \quad \forall\, k,\ k = 1, \cdots, N_S$$

$$(C2) \quad v_F^k(v_I^k, \underline{p}^k, \underline{t}) \leq v_{max}^k, \quad \forall\, k,\ k = 1, \cdots, N_S$$

$$(C3) \quad t_{tr} + \sum_{k=1}^{N_S} t_k \leq T$$

$$(C4) \quad t_k \geq 0, \quad \forall k,\ k = 1, \cdots, N_S$$

$$(C5) \quad \sum_{j=1}^{N_S} x_{ij} = 1, \quad i \neq j; \qquad (C6) \quad \sum_{i=1}^{N_S} x_{ij} = 1, \quad i \neq j$$

$$(C7) \quad \sum_{i,j \in \mathcal{R}} x_{ij} \leq |\mathcal{R}| - 1, \ \ \mathcal{R} \subset \{2, \cdots, N_S\}, |\mathcal{R}| \geq 2$$

$$(C8) \quad x_{ij} = 0 \text{ or } 1$$

UAV Mobility Optimization (Contd.)

- The optimization problem (**P**) can be decomposed into two sub-problems and can be solved in sequential way[65]
- The first sub-problem is stated as,

$$\textbf{(P1):} \quad \underset{x_{ij}}{\text{minimize}} \quad \frac{1}{\mathcal{U}} \sum_{i=1}^{N_S} \sum_{j=1}^{N_S} x_{ij} d_{ij}$$

$$\text{subject to:} \quad (C5),\ (C6),\ (C7),\ \text{and}\ (C8)$$

(P1) evaluates the sequence of visiting the sensor nodes

- The second sub-problem is stated as,

$$\textbf{(P2):} \quad \underset{t_i}{\text{minimize}} \sum_{i=1}^{N_S} t_i$$

$$\text{subject to:} \quad (C1),\ (C2),\ (C3),\ \text{and}\ (C4)$$

(P2) evaluates the optimal charging time of each sensor node

[65] S. Boyd, L. Xiao, A. Mutapcic, and J. Mattingley, "Notes on decomposition methods", *Notes for EE364B, Stanford University*, pp. 1–36, 2007.

UAV Mobility Optimization (Contd.)

Optimal Solution of Problem P1

- UAV wants to minimize the total distance travelled or total travel time of the process while deciding the order of charging
- The known method of shortest visit time computation is *Traveling Salesman Problem (TSP)*[66]

Optimal Solution of Problem P2

- The final voltage of supercapacitor after constant power charging/discharging depends on *charging/discharging rate, time of charging, initial voltage*[67]:
- The charging/discharging equation involves *Lambert function*, which is *analytically intractable* ⇒ *approximation* method required

[66] E. L. Lawler, J. K. Lenstra, A. H. G. R. Kan, and D. B. Shmoys, *The traveling salesman problem: a guided tour of combinatorial optimization*. John Wiley & Sons New York, 1985.

[67] D. Mishra and S. De, "Effects of practical rechargeability constraints on perpetual RF harvesting sensor network operation", *IEEE Access*, vol. 4, pp. 750–765, 2016.

UAV Mobility Optimization (Contd.)

Curve fitting technique

- The final voltage level for charging of supercapacitor is found to fit as a function of initial voltage level, charging rate, and time:

$$v_F(v_I, p_c, t) = v_I + g_c(p_c) \cdot t, \quad g_c(p_c) = g_{co} + g_{c1} \cdot p_c$$

where $g_{co} = 2.711 \times 10^{-6}$ and $g_{c1} = 8.863 \times 10^{-3}$

- The final voltage for discharging of supercapacitor is found to fit as a function of initial voltage level, discharging rate, and time:

$$v_F(v_I, -p_d, t) = v_I + g_d(p_d) \cdot t, \quad g_d(p_d) = g_{do} + g_{d1} \cdot p_d$$

where $g_{do} = 1.522 \times 10^{-9}$ and $g_{d1} = -0.01054$

These approximations transform (**P2**) into a linear program

UAV Mobility Optimization (Contd.)

- The three operational regions of a sensor node are categorized as:
  healthy, unhealthy, dead
- *The sequence in which sensor nodes should be charged by UAV such that the unhealthy state of sensor nodes can be avoided*
- Three different charging schemes are presented by considering the sensor nodes' health parameter

Voltage-aware Charging Sequence (VCS)

Operational Time-aware Charging Sequence (TCS)

Iterative Charging Sequence (ICS)

Some Optimization Results

- CO gas sensor having average energy dissipation rate 0.05 mW, i.e., $p_{d_i} = 0.05$ mW $\forall i$ in case of homogeneous sensor deployment[68]
- Numerical values of different parameters for simulation: $P_{tx} = 4$ W, $f = 0.915$ GHz, $P_o = -12$ dBm, $G_{tx} = 2.10$dBi, $G_{rx} = 1.25$dBi, $T = 24$ hrs, $\mathcal{U} = 10$ m/s.

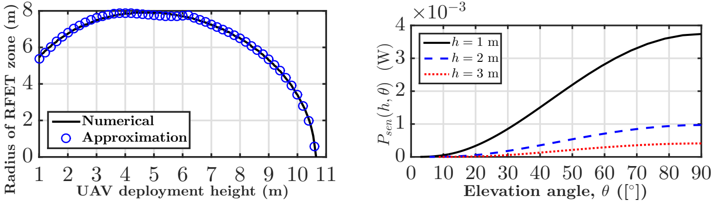

(a) RFET zone (b) power harvested

Figure 7: Variation of (a) radius of RFET zone against UAV deployment height, and (b) effective power available against elevation angle

The radius becomes zero after a particular maximum height, which is the maximum possible height over which UAV can facilitate RFET.

[68] S. Suman, S. Kumar, and S. De, "UAV-assisted RF energy transfer", in *Proc. IEEE Int. Conf. Commun. (ICC)*, Kansas City, MO, USA, 2018, pp. 1–6.

Some Optimization Results (Contd.)

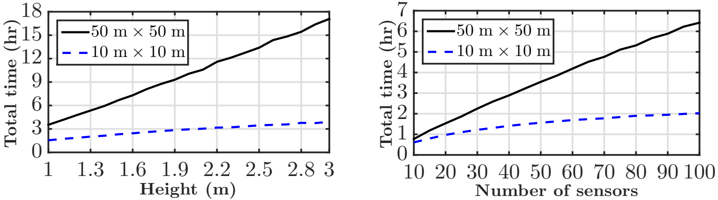

Figure 8: Variation of total charging time against UAV height with $N_S = 50$, and against N_S with $h = 1$ m

Performance of TSP is worst among all schemes

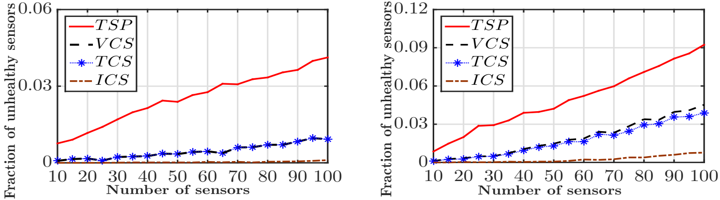

(a) Homogeneous (b) Heterogeneous

Figure 9: Variation of fraction of unhealthy sensor nodes for homogeneous and heterogeneous sensor deployment in 50 m × 50 m area with $h = 1$ m

Hovering Inaccuracy

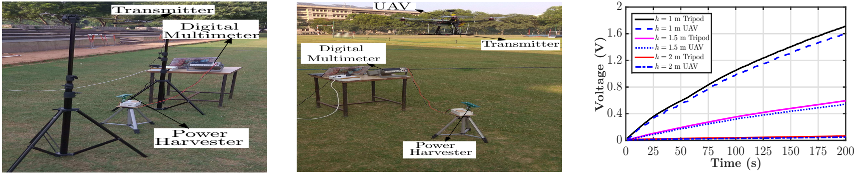

(a) tripod-based set up (b) UAV-based set up (c) voltage variation

Figure 10: Experimental set up for air-to-ground RFET

UAV-aided RFET harvests less energy than tripod-based RFET

Hovering Inaccuracy (Contd.)

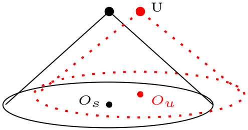

Figure 11: Depiction of hovering inaccuracy

- UAV hovers above different location due to positioning error
- UAV undergoes rotation at this erroneous location
- O_s: position of sensor node having longitude L_o^s and latitude L_a^s
  Let $O_s \equiv (x_s, y_s, 0)$
- O_u: position above which UAV hovers with longitude L_o^u and latitude L_a^u
  Let $O_u \equiv (x_u, y_u, 0)$
- The co-ordinate of UAV at a hovering altitude h: $U \equiv (x_u, y_u, h)$
- This leads to two types of mismatches:
  - Localization Mismatch (LM)
  - Orientation Mismatch (OM)

Localization Mismatch

- The transformation from longitude and latitude to Cartesian coordinate[69]:

$$x_s = R_e \cdot \cos(L_a^s) \cdot \cos(L_o^s),\ x_u = R_e \cdot \cos(L_a^u) \cdot \cos(L_o^u)$$

$$y_s = R_e \cdot \cos(L_a^s) \cdot \sin(L_o^s),\ y_u = R_e \cdot \cos(L_a^u) \cdot \sin(L_o^u)$$

  where $R_e = 6378136.047$ m is radius of the earth.

- Thus, the shift along x-axis and y-axis due to localization mismatch are,

$$x_l = x_u - x_s, \quad y_l = y_u - y_s$$

- The distance between transmitter and receiver d is,

$$d = \sqrt{x_l^2 + y_l^2 + h^2}$$

- The elevation angle (at UAV) Φ_{LM} between sensor node and transmitter,

$$\Phi_{LM} = \arctan\left[\sqrt{(x_l)^2 + (y_l)^2}/h\right]$$

[69] C. T. Russell, "Geophysical coordinate transformations", *Cosmic Electrodynamics*, vol. 2, no. 2, pp. 184–196, 1971.

Orientation Mismatch

- UAV undergoes rotation due to angular displacement while hovering
- UAV-mounted antenna orientation changes due to angular displacement

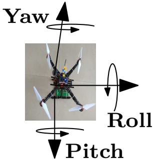

Figure 12: Depiction of three rotational axes of UAV

- Three types of rotational motion[70]: *Pitch*, *Roll*, and *Yaw*
  - *Pitch*: rotation around the lateral axis
  - *Roll*: rotation around the longitudinal axis
  - *Yaw*: rotation around the vertical plane of the UAV

[70] J. D. Barton, "Fundamentals of small unmanned aircraft flight", *Johns Hopkins APL Technical Digest*, vol. 31, no. 2, pp. 132–149, 2012.

Orientation Mismatch (Contd.)

- *Roll*: x-axis, *Pitch*: y-axis, *Yaw*: z-axis

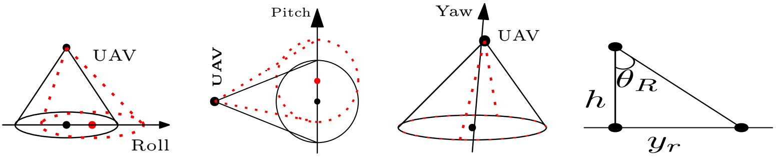

Figure 13: Depiction of impact of rotation.

- If rotation around *Pitch* (*Roll*) is θ_P (θ_R), then the center of beam spot shifts by distance r_P (r_R)

$$\tan\theta_P = \frac{r_P}{h} \Rightarrow r_P = h\cdot\tan\theta_P, \ \Rightarrow r_R = h\cdot\tan\theta_R, \ \theta_P, \theta_R \in [-\frac{\pi}{2}, \frac{\pi}{2}]$$

- The elevation angle (at UAV) Φ_{OM} between the sensor node's antenna and transmitter:

$$\Phi_{OM} = \arctan\left[\sqrt{r_P^2 + r_R^2}/h\right]$$

Effect of Both Mismatches

- The distance between transmitter and receiver remains the same as with *localization mismatch*

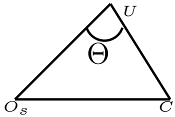

Figure 14: Depiction of effect of both mismatches

- $C \equiv (x_c, y_c, 0)$: shifted center of beam spot due to both mismatches

$$C \equiv (x_c, y_c, 0) \equiv (x_u + r_R, y_u + r_P, 0)$$

- The elevation angle at UAV, Θ between shifted beam center and sensor node is,

$$\Theta = \arccos\left[(\overrightarrow{UO_s} \cdot \overrightarrow{UC})/(|\overrightarrow{UO_s}| \cdot |\overrightarrow{UC}|)\right]$$

where $\overrightarrow{UO_s} = [x_s - x_u, y_s - y_u, -h]$,
$\overrightarrow{UC} = [x_c - x_u, y_c - y_u, -h]$,
$\overrightarrow{UO_s} \cdot \overrightarrow{UC}$ denotes the dot product

Performance with Hovering Inaccuracy

- The transmitter[71] is mounted at the bottom of UAV

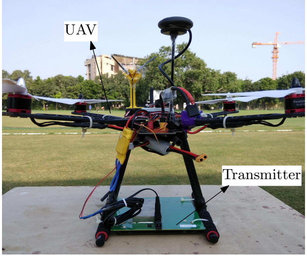

Figure 15: Experimental set up.

- The UAV along with transmitter mounted on it hovers at different altitude: 1 m to 5 m
- The data of GPS location and rotational motion parameter are considered

[71] Powercast, [Online]. Available: http://www.powercastco.com.

Performance with Hovering Inaccuracy (Contd.)

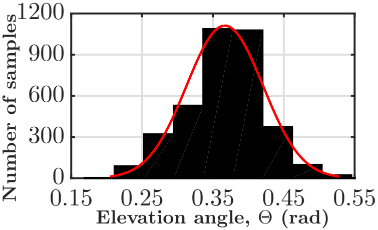

Figure 16: Histogram of Θ, $h = 1$ m.

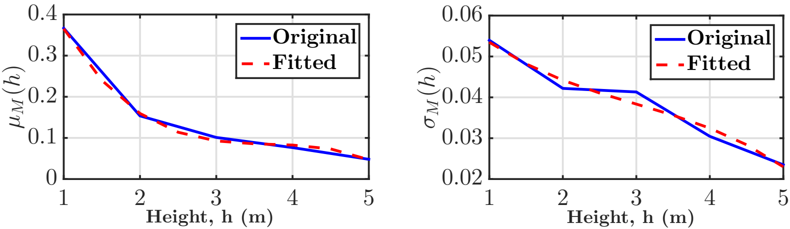

Figure 17: Variation of mean and standard deviation of Θ against height.

Performance with Hovering Inaccuracy (Contd.)

Table 2: Variation of different parameters of hovering inaccuracy

Localization Mismatch	**Distance:** $d(h) = \sqrt{u_1 h^2 + u_2 h + u_3}$ $u_1 = 1.015, u_2 = -0.1193, u_3 = 0.2588,$ **Elevation angle:** $\Phi_{LM}(h) = v_1 h^3 + v_2 h^2 + v_3 h + v_4$ v_1=$-0.01573, v_2$=$0.1763, v_3$=$-0.651, v_4$=$0.8488.$
Orientation Mismatch	**Elevation angle:** $\Phi_{OM}(h) \sim \mathcal{N}(\mu_{OM}(h), \sigma^2_{OM}(h)),$ $\mu_{OM}(h) = w_1 h^3 + w_2 h^2 + w_3 h + w_4$ w_1=$0.00125, w_2$=$-0.01073, w_3$=$0.01871, w_4$= $0.0623,$ $\sigma_{OM}(h) = z_1 h^3 + z_2 h^2 + z_3 h + z_4$ z_1=$-0.001128, z_2$=$0.009966, z_3$=$-0.03044, z_4$=$0.06542.$
Both Mismatch	**Elevation angle:** $\Theta(h) \sim \mathcal{N}(\mu_M(h), \sigma^2_M(h)),$ $\mu_M(h) = a_1 h^3 + a_2 h^2 + a_3 h + a_4$ a_1=$-0.01371, a_2$=$0.1518, a_3$=$-0.5653, a_4$=$0.7925,$ $\sigma_M(h) = b_1 h^3 + b_2 h^2 + b_3 h + b_4$ b_1 =$-0.000584, b_2$=$0.00523 b_3$=$-0.0209, b_4 = 0.06973.$

System Model

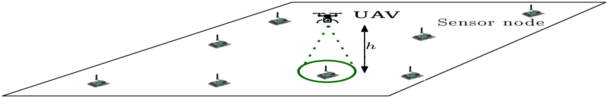

Figure 18: System model for UAV-aided RFET

- UAV visits each sensor node and transfers energy wirelessly
- In this operation, the target sensor node experiences hovering inaccuracy
- The power received at a sensor node when UAV hovers at altitude h is:

$$P_{rx}(h, n, \theta) = P_{tx} \cdot G_0 \cdot g(n, \theta) \cdot (1/d_{tx-rx})^2,$$

where P_{tx}: power transmitted by transmitter mounted on UAV
G_0: Friis equation parameter
$g(n, \theta)$: radiation pattern of transmitter antenna mounted on UAV
n: antenna exponent
θ: elevation angle (at UAV) between transmitter and receiver
d_{tx-rx}: distance between transmitter and receiver

System Model (Contd.)

- The generalized radiation pattern $g(n, \theta)$ of transmitter antenna is[72],

$$g(n, \theta) = 2 \cdot (n + 1) \cdot \cos^n(\theta)$$

- For analytical tractability, the value of antenna exponent n is confined to be integer numbers only
- Thus, $\cos^n \theta$ is

$$\cos^n \theta = \begin{cases} \frac{1}{2^{n-1}} \left[\sum_{r=0}^{\frac{n}{2}-1} \binom{n}{r} \cos((n - 2r)\theta) \right] + \frac{1}{2^n} \binom{n}{n/2}, & \text{if } \; n = \text{even} \\ \frac{1}{2^{n-1}} \left[\sum_{r=0}^{\frac{n-1}{2}} \binom{n}{r} \cos((n - 2r)\theta) \right], & \text{if } \; n = \text{odd} \end{cases}$$

[72] C. A. Balanis, *Antenna Theory: Analysis and Design*. John Wiley & Sons, Inc, 2005.

Characterization of Hovering Inaccuracy

Case 1: No Hovering Inaccuracy (Ideal):

- Here, UAV hovers just above the sensor node and does not undergo rotation at this location
- The received power at the sensor node is

$$P_{rx}^{(1)}(h,n) = P_{tx} \cdot G_0 \cdot g(n,\theta) \cdot \left(\frac{1}{d_{tx-rx}}\right)^2 \Bigg|_{\theta=0, d_{tx-rx}=h}$$
$$= P_{tx} \cdot G_0 \cdot W_1(h,n),$$

where $W_1(h,n)$ is given as,

$$W_1(h,n) = 2(n+1) \cdot \frac{1}{h^2}$$

Characterization of Hovering Inaccuracy (Contd.)

Case 2: Only Localization Mismatch (LM):

- Here, UAV hovers above slightly different position other than the desired one, and does not undergo rotation at this location
- The received power at the sensor node is

$$\begin{aligned} P_{rx}^{(2)}(h,n) &= P_{tx} \cdot G_0 \cdot g(n,\theta) \cdot (1/d_{tx-rx})^2 \Big|_{\theta=\Phi_{LM}(h), d_{tx-rx}=d(h)} \\ &= P_{tx} \cdot G_0 \cdot W_2(h,n) \end{aligned}$$

where $W_2(h,n)$ is

$$W_2(h,n) = 2(n+1) \cdot \cos^n(\Phi_{LM}(h)) \cdot 1/d^2(h)$$

Lemma 8

$W_2(h,n)$ is unimodal function of hovering altitude h for a given antenna exponent.

Lemma 9

$W_2(h,n)$ is a unimodal function of antenna exponent n for a given hovering altitude.

Characterization of Hovering Inaccuracy (Contd.)

Case 3: Only Orientation Mismatch (OM):

- Here, UAV hovers above the desired position and undergoes rotation at this location
- The received power at the sensor node

$$P_3(h,n,\theta) = P_{tx} \cdot G_0 \cdot g(n,\theta) \cdot (1/d_{tx-rx})^2 \Big|_{\theta=\Phi_{OM}(h), d_{tx-rx}=h}$$

- It may be noted that, elevation angle $\Phi_{OM}(h)$ is a random variable and follows Gaussian distribution
- The received power in expected sense is a correct metric for performance evaluation

$$\begin{aligned} P_{rx}^{(3)}(h,n) &= \mathbb{E}\left[P_3^{rx}(h,n,\theta)\right] \\ &= P_{tx} \cdot G_0 \cdot \left(\frac{1}{h}\right)^2 \int_{-\infty}^{\infty} g(n,\theta) \cdot f_{\Phi_{OM}(h)}(\theta) \cdot d\theta \end{aligned}$$

Characterization of Hovering Inaccuracy (Contd.)

If $\mathcal{X} \sim \mathcal{N}(\mu_{\mathcal{X}}, \sigma_{\mathcal{X}})$ is a Gaussian random variable. Its characteristic function:

$$\Psi_{\mathcal{X}}(\tau) = \mathbb{E}[\exp(i\tau\mathcal{X})] = \exp(i\tau\mu_{\mathcal{X}} - \frac{1}{2}\sigma_{\mathcal{X}}^2\tau^2)$$

Then $\mathbb{E}[\cos(\tau\mathcal{X})] = \cos(\mu_{\mathcal{X}}\tau) \cdot \exp(-\frac{1}{2}\sigma_{\mathcal{X}}^2\tau^2)$

Using the expression of $\cos^n(\theta)$ and $\mathbb{E}[\cos(\tau\mathcal{X})]$, $P_{rx}^{(3)}(h,n)$ is written as

$$P_{rx}^{(3)}(h,n) = P_{tx} \cdot G_0 \cdot W_3(h,n)$$

where $W_3(h,n)$ is

$$W_3(h,n) = \frac{1}{h^2} \cdot \begin{cases} X_{even}(h,n), & \text{if } \; n = \text{even} \\ X_{odd}(h,n), & \text{if } \; n = \text{odd} \end{cases}$$

with $X_{even}(h,n) = \frac{1}{2^{n-1}} \Big[\sum_{r=0}^{\frac{n}{2}-1} \binom{n}{r} \cos((n-2r)\mu_{OM}(h)) \exp\Big(-\frac{1}{2}(n-2r)^2\sigma_{OM}^2(h)\Big)\Big] + \frac{1}{2^n}\binom{n}{n/2}$

$$X_{odd}(h,n) = \frac{1}{2^{n-1}} \Big[\sum_{r=0}^{\frac{n-1}{2}} \binom{n}{r} \cos((n-2r)\mu_{OM}(h)) \exp\Big(-\frac{1}{2}(n-2r)^2\sigma_{OM}^2(h)\Big]$$

Characterization of Hovering Inaccuracy (Contd.)

Lemma 10

$W_3(h, n)$ is non-increasing function of hovering altitude h for a given antenna exponent.

Lemma 11

$W_3(h, n)$ is non-decreasing of antenna exponent n for a given hovering altitude.

Case 4: Both LM and OM:

- Here, UAV does not hover above the desired position and undergoes rotation at this location
- The received power at the sensor node is

$$P_4(h, n, \theta) = P_{tx} \cdot G_0 \cdot g(n, \theta) \cdot (1/d_{tx-rx})^2 \Big|_{\theta=\Theta(h),\, d_{tx-rx}=d(h)}$$

Characterization of Hovering Inaccuracy (Contd.)

- The received power in expected sense:

$$P_{rx}^{(4)}(h,n) = \mathbb{E}\big[P_4^{rx}(h,n,\theta)\big]$$
$$= P_{tx} \cdot G_0 \cdot \left(\frac{1}{d(h)}\right)^2 \int_{-\infty}^{\infty} g(\theta) \cdot f_{\Theta(h)}(\theta) \cdot d\theta$$

- This can be rewritten as,

$$P_{rx}^{(4)}(h,n) = P_{tx} \cdot G_0 \cdot W_4(h,n)$$

where $W_4(h,n)$ is given as,

$$W_4(h,n) = \frac{1}{d^2(h)} \cdot \begin{cases} Y_{even}(h,n), & \text{if } \ n = \text{even} \\ Y_{odd}(h,n), & \text{if } \ n = \text{odd} \end{cases}$$

with

$$Y_{even}(h,n) = \frac{1}{2^{n-1}}\left[\sum_{r=0}^{\frac{n}{2}-1}\binom{n}{r}\cos((n-2r)\mu_M(h))\exp\left(-\frac{1}{2}(n-2r)^2\sigma_M^2(h)\right)\right] + \frac{1}{2^n}\binom{n}{n/2}$$

$$Y_{odd}(h,n) = \frac{1}{2^{n-1}}\left[\sum_{r=0}^{\frac{n-1}{2}}\binom{n}{r}\cos((n-2r)\mu_M(h))\exp\left(-\frac{1}{2}(n-2r)^2\sigma_M^2(h)\right)\right]$$

Characterization of Hovering Inaccuracy (Contd.)

Lemma 12

$W_4(h, n)$ is unimodal function of hovering altitude h for a given antenna exponent.

Lemma 13

$W_4(h, n)$ is unimodal function of antenna exponent n for a given hovering altitude.

Selection of Optimal System Parameters

- Aim: maximize received power by transmitting minimum power
- For this purpose, an optimization problem for k^{th} case is:

$$
\begin{aligned}
(\mathbf{P01}):\ & \underset{h,n}{\text{minimize}} \quad P_{tx}^{(k)} \\
\text{s. t.: } (\mathbf{C1}):\ & P_{rx}^{(k)}(h,n) \geq P_{sat} \\
(\mathbf{C2}):\ & h_{min} \leq h \leq h_{max} \\
(\mathbf{C3}):\ & n_{min} \leq n \leq n_{max}
\end{aligned}
$$

- **(P01)** selects the optimal system parameters:
  transmit power (P_{opt}^{tx}), hovering altitude (h_{opt}), antenna exponent (n_{opt})
- Variable of **(P01)** are continuous (P_k^{tx}, h) as well as discrete (n)
- Using the nature of $W_k(h,n)$ proved in Lemma 4 - 9, an algorithm is proposed to find the optimal system parameters
- P_{sat} is saturation region of power harvester

Selection of Optimal System Parameters (Contd.)

Algorithm 1 Optimal Design with Hovering Inaccuracy Algorithm

if $k = 1$ or $k = 3$ **then**
  $h_{opt} = h_{min}, n_{opt} = n_{max}$; calculate $W_k(h_{opt}, n_{opt})$
  $P_{opt}^{tx} = P_0/G_0 \cdot W_k(h_{opt}, n_{opt})$
end if
if $k = 2$ or $k = 4$ **then**
  $\Delta = 1, n = n_{min}$
  Calculate $h^*(n)$ for given n using *golden-section method*
  Calculate $W_k(h^*(n), n)$
  while $\Delta \geq 0$ **do**
    $n = n + 1$
    Calculate $h^*(n)$ for given n using *golden-section method*
    Calculate $W_k(h^*(n), n)$
    $\Delta = W_k(h^*(n), n) - W_k(h^*(n-1), n-1)$
  end while
  $n_{opt} = n - 1, h_{opt} = h^*(n-1), P_{opt}^{tx} = P_0/G_0 \cdot W_k(h_{opt}, n_{opt})$
end if

Optimization Results with Hovering Inaccuracy

Numerical values of different parameters for simulation:

$P_{tx} = 1$ W, $G_{rx} = 2.10$, $P_o = 45$ mW, $n_{min} = 1$, $n_{max} = 50$,
$h_{min} = 1$ m, $h_{max} = 3$ m , $\lambda = 0.32786$ cm (frequency is 0.915 GHz)

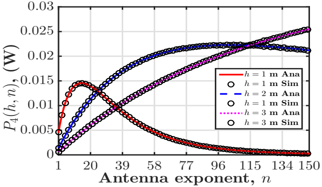

Figure 19: Variation of received power against antenna parameter with *LM and OM*

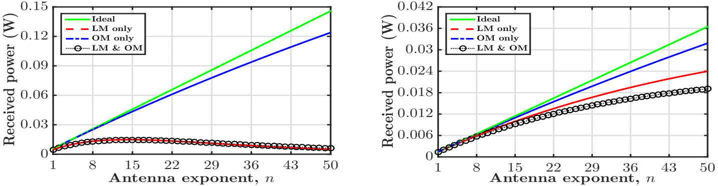

(a) $h = 1$ m (b) $h = 2$ m

Figure 20: Variation of received power for different cases against antenna exponent

Optimization Results with Hovering Inaccuracy (Contd.)

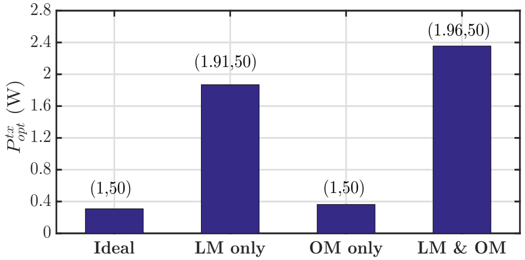

Figure 21: Variation of optimal system parameters for different cases

Impact of LM is more severe than OM

Concluding Remarks

- Path loss model for UAV-aided RFET is presented
- RFET Zone is conceptualized and power harvested at sensor node is obtained
- An optimization problem is formulated to obtain the charging time and visiting sequence
- A framework to analyze the hovering inaccuracy of UAV is presented
- The performance in presence of hovering inaccuracy is investigated
- Optimal system parameters (transmit power, altitude, antenna) are estimated

Queries

IITD-CNRG Website:
http://cnrg.iitd.ac.in/
Contact: swadesd@ee.iitd.ac.in

Thanks!